

DRAFT VERSION AUGUST 20, 2025

Typeset using L^AT_EX modern style in AASTeX63

CGM cloud sizes from refractive FRB scattering

LLUÍS MAS-RIBAS,^{1,2} MATTHEW MCQUINN,³ AND J. XAVIER PROCHASKA^{1,2,4,5}

¹*Department of Astronomy and Astrophysics, University of California, 1156 High Street, Santa Cruz, CA 95064, USA*

²*University of California Observatories, 1156 High Street, Santa Cruz, CA 95064, USA*

³*Department of Astronomy, University of Washington, Seattle, WA 98195-1580, USA*

⁴*Kavli Institute for the Physics and Mathematics of the Universe (Kavli IPMU), 5-1-5 Kashiwanoha, Kashiwa, 277-8583, Japan*

⁵*Division of Science, National Astronomical Observatory of Japan, 2-21-1 Osawa, Mitaka, Tokyo 181-8588, Japan*

ABSTRACT

We explore constraints on the size of cool gas clouds in the circumgalactic medium (CGM) obtainable from the presence, or lack thereof, of refractive scattering in fast radio bursts (FRBs). Our refractive analysis sets the most conservative bounds on parsec-scale CGM clumpiness as it does not make assumptions about the turbulent density cascade. We find that the bulk of low-redshift cool CGM gas, constrained to have densities of $n_e \lesssim 10^{-2} \text{ cm}^{-3}$, likely cannot produce two refractive images and, hence, scattering. It is only for extremely small cloud sizes $\lesssim 0.1 \text{ pc}$ (about a hundred times smaller than the so-called shattering scale) that such densities could result in detectable scattering. Dense $n_e \gtrsim 0.1 \text{ cm}^{-3}$ gas with shattering-scale cloud sizes is more likely to inhabit the inner several kiloparsecs of the low-redshift CGM: such clouds would result in multiple refractive images and large scattering times $\gtrsim 1 - 10 \text{ ms}$, but a small fraction of FRB sightlines are likely to be affected. We argue that such large scattering times from an intervening CGM would be a signature of sub-parsec clouds, even if diffractive scattering from turbulence contributes to the overall scattering. At redshift $z \sim 3$, we estimate $\sim 0.1\%$ of FRBs to intersect massive proto-clusters, which may be the most likely place to see scattering owing to their ubiquitous $n_e \approx 1 \text{ cm}^{-3}$ cold gas. While much of our discussion assumes a single cloud size, we show similar results hold for a CGM cloud-size distribution motivated by hydrodynamic simulations.

1. INTRODUCTION

Fast radio bursts (FRBs) are luminous millisecond-duration radio pulses of yet an unclear origin (Petroff et al. 2022), arising from a variety of galactic environments, and from dwarf to massive galaxies (e.g., Mannings et al. 2021; Bhardwaj et al. 2023; Hewitt et al. 2024; Shah et al. 2024; Eftekhari et al. 2024; Sharma et al. 2024). Because FRBs are extragalactic sources, currently detected up to $z \gtrsim 1$ (Ryder et al. 2023), they can be used to probe the media intersected by their light on its way from the source to our telescopes (McQuinn 2014; Prochaska et al. 2019; Macquart et al. 2020; Simha et al. 2020; Lee et al. 2022; Baptista et al. 2023; Simha et al. 2023; Lee et al. 2023; Connor et al. 2024; Khrykin et al. 2024).

Of particular interest here is the potential to study the circumgalactic medium (CGM) in intervening halos along the line-of-sight to FRBs. The CGM is the gaseous region extending out to a few hundreds of kiloparsecs around galaxies, connecting the intergalactic (IGM) and interstellar (ISM) media. It is a multiphase environment in which cool ($T \sim 10^4$ K) gas clouds are embedded in a more diffuse and hotter ($T \sim 10^6$ K) component, but the detailed features of this cool gas remain unknown (see Tumlinson et al. 2017; Faucher-Giguere & Oh 2023, for reviews). Low-ionization metal transitions in the spectra of quasar sightlines intersecting the CGM indicate that the cool gas has an almost unity areal covering fraction (Chen et al. 2010; Nielsen et al. 2013; Werk et al. 2013; Dutta et al. 2020; Huang et al. 2021), with a smaller ($\lesssim 10\%$) volume filling fraction (Stocke et al. 2013; Werk et al. 2014; Stern et al. 2016; Faerman & Werk 2023). Furthermore, the line width of these metal lines ($\sim 10\text{--}50$ km s $^{-1}$; Werk et al. 2013; Qu et al. 2022) probes the velocity structure of the gas, but it is still unclear whether these widths are set by the turbulent velocity within a single cloud or from the velocity dispersion of many small independent clouds.

The sizes of the CGM clouds carry information about the physical processes responsible for the multiphase structure, but this quantity is difficult to constrain observationally. Sizes of absorption *systems* of $\sim 1\text{--}10$ kpc have been probed from multiply lensed quasars (Rauch et al. 2001; Ellison et al. 2004; Rubin et al. 2018b; Kulkarni et al. 2019; Augustin et al. 2021; Dutta et al. 2024, and similarly from the sightlines to background galaxies; Lopez et al. 2018; Péroux et al. 2018; Rubin et al. 2018a; Tejos et al. 2021), and coherent scales down to a few hundred pc were inferred with quasar sightline pairs by, e.g., Rauch et al. (2001) and Rudie et al. (2019). Furthermore, a median cloud size of ~ 100 pc in the CGM of (quiescent) luminous red galaxies was inferred by Zahedy et al. 2019 (see also Zahedy et al. 2021) through photoionization modeling, with their data covering the range $\sim 10\text{--}10^4$ pc. Chen et al. (2023) performed a similar analysis to that of Zahedy et al. (2019) including star-forming galaxies and found a wider range of sizes that extend to clouds of ~ 1 pc. Finally, it is worth noting the large population of so-called high-velocity clouds (HVC) inhabiting the inner ~ 10 kpc of the Milky Way halo (Wakker et al. 2008), with a small fraction of them also found at large Galactic distances (several tens of kpc), as well as in

the CGM of Andromeda (Putman et al. 2003; Pisano et al. 2007). HVCs are often detected in 21 cm and H α emission, and they show self-similar (fractal) structure down to the spatial resolution of observations (Vogelaar & Wakker 1994), which may indicate very small cloud sizes (see also Wakker & van Woerden 1997; Putman et al. 2012, for reviews).

From the theoretical side, there has recently been substantial work on the potential for parsec-scale clouds at $\sim 10^4$ K condensing from hot gas. McCourt et al. (2018) pointed out that a very natural scale for the gas to clump is the sound speed times the cooling time, at least in the plausible limit where conduction is highly suppressed by magnetic fields. They found in hydrodynamic simulations that cooling gas tends to fragment on this ‘shattering’ scale. Others have found that even if the gas does not shatter, it may ‘splatter’ and form cloudlets at the shattering scale if it reaches the $\sim 10^4$ K equilibrium temperature with supersonic inward velocities (Waters & Proga 2023; Farber & Gronke 2023). While linear perturbations to virialized gas may not shatter because of thermal instability (Waters & Proga 2023), nonlinear perturbations in the virialized gas can break up on the shattering scale (Gronke & Oh 2020). If formed, it is then possible that the small cloudlets re-coagulate into larger clouds as found in Das et al. (2021) and Gronke et al. (2022). We will consider the results of the simulations of Gronke et al. (2022) that find that such coagulation results in a power-law distribution of cloud sizes.

Various physical quantities that characterize the intervening CGM can be obtained from FRB observables. For example, the total column density of free electrons traversed by the radio signal, the so-called dispersion measure (DM), induces a delay in the arrival time of the photons that has a characteristic frequency dependence of ν^{-2} . Thus, the modeling of this dependence allows us to infer the electron column of all the media intersected by the radio waves. When the dispersion measure is weighted by the parallel component of the magnetic field in the medium along the FRB sightline, one obtains the quantity referred to as Faraday rotation measure (RM), related to the polarization of the radiation. Furthermore, the scattering of photons by the intersected medium gives rise to additional effects: scattering breaks up an FRB into multiple images, resulting in an observed angular broadening of the source. The arrival of these images at the observer location at different times (with time delays that depend on frequency as ν^{-4}) results in their temporal superposition, which may yield to an overall extended signal dubbed scatter broadening (Williamson 1972). These multiple images can also interfere with one another, an effect known as scintillation, where intensity fluctuations appear in the observed FRB spectrum. The existence and characteristics of the scatter broadening and scintillation signals depend on the physical properties of the intervening gas (its density and cloud sizes), as well as on its location along the sightline with respect to the FRB source and the observer (e.g., Narayan 1992, see also Ginzburg 1970; Draine 2011; Cordes & Chatterjee 2019). Limits on the distance to the gas responsible for the scattering (addressing whether

this gas is near the FRB source or further along the sightline) from the presence of scintillation from gas within the Milky Way have been addressed in previous work (e.g., Masui et al. 2015; Sammons et al. 2023; Nimmo et al. 2024), while here we will focus on the constraints on the cloud sizes and density of the intervening CGM gas.

Scattering of radio waves is often categorized by taking into account the size of the scatterers. Diffractive scattering comprises the regime where the scatterers are below the Fresnel scale and thus lead to light taking multiple interfering paths. This is generally thought to occur from density fluctuations driven by turbulence (e.g., Rickett 1990), as turbulence can lead to a cascade that reaches extremely small length scales. Turbulence is the canonical source for scattering in the Milky Way interstellar medium (Armstrong et al. 1995), although it is likely that other interstellar structures lead to at least some of the more extreme scattering events (Pen & Levin 2014). For the case of a CGM at a distance of one gigaparsec, the scale of fluctuations below which scattering becomes diffractive is approximately an astronomical unit (Prochaska et al. 2019). Turbulence could lead to fluctuations on such small scales and indeed is observed to have structure on thousands of kilometer scales in the ISM. However, the details of the turbulence that can lead to fluctuations on diffractive scales is hotly debated (e.g. Schekochihin 2022). Even in the context of Goldreich & Sridhar (1995) MHD turbulence, Prochaska et al. (2019, see the supplementary documents) stresses that various physical processes can result in the cut-off of the density spectrum in the density cascade prior to the diffractive scale. For example, turbulent density fluctuations may not be passively advected by the flow to small eddies if the cascade becomes isothermal prior to eddies where transport is set by magnetic waves, and there may additionally be a cutoff from proton free streaming/diffusion that can be larger than the diffractive scale (Lithwick & Goldreich 2001). Such cut-offs in the turbulent cascade would suppress or eliminate diffractive scattering.

Refractive scattering, on the other hand, considers scatterers larger than the Fresnel scale. It is particularly sensitive to discrete CGM clouds of sizes of $\lesssim 1$ pc (Vedantham & Phinney 2019). As discussed above, these sizes are challenging to probe with other observational methods, but they are potentially consistent with absorption-line spectroscopy results if each absorption system is composed of thousands of parsec-scale clouds (e.g., Werk et al. 2016; McQuinn & Werk 2018; Faerman et al. 2024a) as has been conjectured (McCourt et al. 2018). Refraction is also interesting because it potentially leads to the largest scattering times: We will argue that it is challenging to produce diffractive scattering from CGM turbulence that is significantly larger than our estimates for refractive scattering from clouds.

Finally, we point out that for the low- z CGM, the typical inferred densities are such that the shattering scale is likely tens or hundreds of parsecs. Thus, even if the CGM does shatter and result in such cloud sizes, these clouds are too large to produce refractive scattering. This contrasts with the findings of previous studies,

which suggest that FRB scattering places strong limits on low-redshift scattering-scale cloudlets (Vedantham & Phinney 2019; Jow et al. 2023).

In this paper, we investigate the constraints on the size of cool CGM gas clouds that can be obtained from refractive scattering, and discuss these effects and results in the context of actual CGM observations. Section 2 presents the refraction formalism, adopting part of the methods in Jow et al. (2023) who explored similar constraints for sub-parsec cloudlets via a combined plasma and lensing approach. A fiducial toy model halo is used in Section 3 to infer dependencies on halo parameters and to obtain general results. In Section 4, we explore variations of the fiducial halo and alternate physical scenarios motivated by observations and simulations. We compare the contributions of refractive and diffractive CGM scattering in Section 5, and conclude in Section 6.

2. FORMALISM

Section 2.1 below describes the formalism for refractive scattering in the circumgalactic medium of extragalactic halos. The impact of extragalactic refractive scattering on Milky Way scintillation is then presented in Section 2.2.

2.1. Refractive Scattering

The (rest-frame) plasma frequency is

$$\nu_p = \sqrt{\frac{e^2 n_e}{4\pi^2 \epsilon_0 m_e}}, \quad (1)$$

where m_e and e are the electron mass and charge, respectively, n_e is the electron density of the medium, and ϵ_0 is the vacuum permittivity¹. Regions in the plasma with fluctuations Δn_e departing from the mean electron density translate into root mean square fluctuations of the refractive index (Draine 2011, chapter 11)

$$\Delta m_{\text{rest}} = \frac{1}{2} \frac{\omega_p^2}{\omega_{\text{rest}}^2} = \frac{e^2}{2\epsilon_0 m_e \omega_{\text{rest}}^2} \Delta n_e, \quad (2)$$

which induce phase velocity variations $\Delta v_{\text{phase}} = c \Delta m_{\text{rest}}$ of the radio waves propagating through such a medium. Here and in the following, $\omega_{\text{rest}} = 2\pi\nu_{\text{rest}}$ ($\omega_p = 2\pi\nu_p$) is the rest-frame angular frequency of the radio waves (plasma) and c denotes the speed of light. These effects, in turn, result in a shift of the wave phase

$$\Delta x_c = l \Delta m_{\text{rest}}, \quad (3)$$

where $l = 2r_c$ is the path length that the radio waves traverse when encountering one region (cloud), which we will consider spherical with radius r_c . Here, l implies that the region is intersected through its center.

¹ The term $4\pi\epsilon_0$ in the denominator equals unity in cgs units often used in astronomy. We explicitly write this term (in SI units) in all our expressions for clarity.

For pairs of rays separated by a distance $2r_c$, such that they have independent paths, the difference in their phases results in a distortion of the wavefront, corresponding to a change in the direction of propagation of the radio waves by an angle (see Figure 11.6 in [Draine 2011](#), for a schematic representation)

$$\alpha_c \approx g_s \frac{\sqrt{2} \Delta x_c}{2 r_c} = g_s \sqrt{2} \Delta m_{\text{rest}} , \quad (4)$$

where $g_s = 2.2$ is a geometric correction factor computed by [Prochaska et al. \(2019\)](#) that applies for perfectly spherical clouds².

In a medium consisting of many clouds, such as a galaxy halo, this angle is

$$\alpha \approx \sqrt{\sum_j^{N_c} \alpha_{c,j}^2} = g_s \sqrt{2 N_c} \Delta m_{\text{rest}} , \quad (5)$$

where N_c is the number of clouds intersected by a ray and, since we now explicitly account for the number of clouds in the expressions, the term Δm_{rest} simply refers to a single cloud of density n_e .

With the expressions derived above and considering cosmological distances, we can now define the scattering angle in the observer frame as (e.g., [Macquart & Koay 2013](#))

$$\Theta_s \approx \frac{d_{\ell s}}{d_s} \alpha = \frac{1}{(1+z_\ell)^2} \frac{d_{\ell s}}{d_s} g_s \sqrt{2 N_c} \Delta m , \quad (6)$$

and the (geometric) scattering time, i.e., the time delay between images formed by refraction, as

$$\tau_s \approx (1+z_\ell) \frac{d_\ell d_s}{d_{\ell s}} \frac{\Theta_s^2}{2c} = \frac{1}{(1+z_\ell)^3} \frac{d_\ell d_{\ell s}}{d_s} g_s^2 \frac{N_c}{c} \Delta m^2 . \quad (7)$$

Here, d_ℓ , d_s , $d_{\ell s}$ are the angular diameter distances ([Peacock 1999](#)) from the observer to the scattering screen (owing to plasma lensing from an intervening CGM), from the observer to the source, and from the scattering screen to the source, respectively. The term z_ℓ denotes the redshift of the screen and Δm is now defined in the observer frame via the observed frequency $\nu(1+z_\ell) = \nu_{\text{rest}}$. Equation 7 highlights the fundamental role played by the number of clouds in the time delay. Specifically, it is the crossing of the radio waves into and out of these higher density media that induces scattering (refraction) and, therefore, the larger the number of clouds, the higher the scattering.

As we will show below, another relevant quantity in our work is the number of images produced by refractive scattering in the CGM (cf. [Prochaska et al. 2019](#); [Jow et al. 2023](#)). We can define this term following [Jow et al. \(2023\)](#) as

$$N_{\text{img}} \sim 1 + N_c k_c^2 , \quad (8)$$

² For slab-like clouds with the same characteristic r_c size, the correction term would simply equate unity, thus spherical clouds represent an upper limit for the angle (and scattering time) values.

where k_c is the lens convergence for a single cloud:

$$k_c = \frac{1}{(1+z_1)^2} \frac{d_1 d_{ls}}{d_s} \frac{\sqrt{2} \Delta m}{r_c} \sim \frac{\Theta_c}{\theta_c}, \quad (9)$$

where $\theta_c = r_c/d_\ell$ and Θ_c are the angular scale and the scattering angle from a single CGM cloud in the intervening halo, respectively. Equation 8 shows that even intersecting a single cloud ($N_c = 1$) can result in more images than the original image of the source, as long as the cloud convergence is $k_c \geq 1$. When the number of clouds is large, as is the case of a halo, however, this condition is relaxed as then only the total column of clouds ($N_c k_c^2$) must be greater than unity to produce multiple images.

2.2. Extragalactic Halos and their Effect on Milky Way Scintillation

One way to probe the impact of refractive scattering from an intervening extragalactic halo is on the FRB scintillation signal created by the Milky Way. We briefly summarize here the aspects of this process that are relevant for our work, and refer the reader to [Jow et al. 2023](#) and [Pradeep et al. 2025](#), for additional discussion and formulation (see also these works for schematic representations of these processes).

Let us first consider scintillation as the result of multipath propagation arising from scattering in the Milky Way ([Rickett 1970](#)). In this scenario, multiple images created by scattering in the Milky Way, and separated by a characteristic time τ_{MW} smaller than the pulse duration, interfere at the observer location giving rise to intensity fluctuations in the FRB spectrum with a characteristic frequency scale of $1/\tau_{\text{MW}}$.

The presence of a distant circumgalactic medium (whether intervening or around the FRB host itself) along the FRB sightline that scatters the signal and creates multiple (i.e., more than one) images with a time delay τ_s , however, may eliminate the Milky Way scintillation signal. For this to happen, the Milky Way scattering screen must resolve the images from the extragalactic CGM (i.e., each image from the halo must appear separated by an angle greater than $\sim \lambda/\sqrt{c\tau_{\text{MW}}d_{\text{MW}}}$, where d_{MW} is the distance to the Milky Way scattering screen and $\lambda = c\nu^{-1}$; [Sammons et al. 2023](#)), otherwise there would be no interference. By using that the separation between images at the CGM lens is $\sqrt{\tau_s c/d_\ell}$, one can then obtain the lower limit for τ_s that enables the MW to resolve the CGM images given τ_{MW} :³

$$\tau_s = 1 \mu\text{s} \left(\frac{d_\ell}{1 \text{ Gpc}} \right) \left(\frac{d_{\text{MW}}}{1 \text{ kpc}} \right)^{-1} \left(\frac{\tau_{\text{MW}}}{1 \mu\text{s}} \right)^{-1} \left(\frac{\nu}{1 \text{ GHz}} \right)^{-2}. \quad (10)$$

The larger the scattering time in the halo compared to the value required from the above expression, the more suppression of the Milky Way scintillation signal ([Pradeep et al. 2025](#)). We stress that the number of images must be $N_{\text{img}} \geq 2$ to have a defined scattering time and for this effect to happen.

³ Here we have omitted cosmological distances for simplicity. Formal expressions accounting for this effect are derived in [Pradeep et al. \(2025\)](#) and appendix B in [Sammons et al. \(2023\)](#).

In the following sections, we will use the expressions for the time delay and number of images derived above to explore the constraints that can be obtained for intervening halos and the contribution of refraction to the overall scattering signal.

3. A TOY MODEL HALO OF SINGLE-SIZE CLOUDS

We consider here the case of an extragalactic halo consisting of an ensemble of cool clouds of the same size and density, embedded in a more diffuse and warmer medium. These clouds represent the cool CGM medium that is observed in absorption in quasar spectra, and we ignore the contribution of the warm component assuming that its density, and thus scattering, is much lower than that of the cool gas (Ocker et al. 2025). This simple approach will allow us to gain broad insight into the dependence of the refractive scattering time delay and number of images on the cloud size and other halo parameters, as well as into the impact of scattering on scintillation and/or pulse broadening.

We begin by considering a CGM with a constant radial volume filling fraction of cool clouds extending out to the halo virial radius r_{200} , a model that describes observations of the low- z CGM (e.g., Faerman & Werk 2023)⁴:

$$f_v(r) = \begin{cases} f_v & \text{for } r \leq r_{200}; \\ 0 & \text{otherwise} \end{cases} \quad (11)$$

The number of clouds intersected by a sightline traversing this halo at impact parameter b is then

$$N_c(b) = 2 \int_0^{\sqrt{r_{200}^2 - b^2}} \frac{\pi r_c^2}{\frac{4}{3}\pi r_c^3} f_v(\sqrt{s^2 + b^2}) ds = \frac{3}{2} \frac{f_v}{r_c} \sqrt{r_{200}^2 - b^2}, \quad (12)$$

and if we further specialize to $b \ll r_{200}$:

$$N_c(b) \equiv N_c = \frac{3}{2} f_v \frac{r_{200}}{r_c}. \quad (13)$$

With this expression, the dependence of the refractive scattering time delay on halo parameters (in addition to the halo redshift and its location relative to the observer and the source, as well as observed frequency) becomes

$$\tau_s \propto \frac{1}{(1 + z_\ell)^3} \frac{d_\ell d_{\ell s}}{d_s} f_v \frac{r_{200}}{r_c} \frac{n_e^2}{\omega^4}. \quad (14)$$

This expression indicates that the time delay from refractive scattering is proportional to the size of the halo, the volume filling fraction, the square of the electron density in the clouds, and inversely proportional to the cloud size. For the number of (additional)

⁴ These authors assume a constant filling factor but the density of their clouds depends on radial distance as $r^{-1.67}$, while we assume a constant density for simplicity.

images created by refraction, there is a stronger dependence on the geometrical term and, most important, on the cloud size, compared to the time delay case, such that

$$N_{\text{img}} - 1 \propto \frac{1}{(1 + z_\ell)^4} \left(\frac{d_\ell d_{\ell s}}{d_s} \right)^2 f_v \frac{r_{200}}{r_c^3} \frac{n_e^2}{w^4}. \quad (15)$$

Adopting values for a fiducial halo and its CGM (motivated by absorption-line studies), one estimates that the typical refractive time delay between images is

$$\begin{aligned} \tau_s \approx & \frac{2.5}{(1 + z_1)^3} \text{ms} \left(\frac{d_\ell d_{\ell s}/d_s}{1 \text{ Gpc}} \right) \left(\frac{f_v}{0.1} \right) \left(\frac{r_{200}}{200 \text{ kpc}} \right) \\ & \times \left(\frac{n_e}{10^{-2} \text{ cm}^{-3}} \right)^2 \left(\frac{r_c}{1 \text{ pc}} \right)^{-1} \left(\frac{\nu}{1 \text{ GHz}} \right)^{-4} \quad \text{if} \quad N_{\text{img}} \geq 2, \end{aligned} \quad (16)$$

and the number of images:

$$\begin{aligned} N_{\text{img}} - 1 \approx & \frac{10^{-2}}{(1 + z_1)^4} \left(\frac{d_\ell d_{\ell s}/d_s}{1 \text{ Gpc}} \right)^2 \\ & \times \left(\frac{f_v}{0.1} \right) \left(\frac{r_{200}}{200 \text{ kpc}} \right) \left(\frac{n_e}{10^{-2} \text{ cm}^{-3}} \right)^2 \left(\frac{r_c}{1 \text{ pc}} \right)^{-3} \left(\frac{\nu}{1 \text{ GHz}} \right)^{-4}. \end{aligned} \quad (17)$$

Figure 1 shows scattering time delays induced by a halo composed of clouds of size and electron density fluctuations over ranges that cover frequently assumed halo values at low redshift (e.g., [Faerman & Werk 2023](#)), and with the formalism just described above. The panels show two values for the volume filling fraction, for comparison, noting that the highest value (top panel) is favored by the observations of [Werk et al. 2014](#) (i.e., $f_v \sim 10^{-1} - 10^{-2}$). Because we are most interested in the dependence on these parameters here, we have set the values $z_\ell = 0^5$, $r_{200} = 200 \text{ kpc}$ (typical of a Milky Way halo mass $\log(M_h/M_\odot) \approx 12.2$ at $z = 0$, although the cool gas might be contained within a slightly shorter radius), $\nu = 1 \text{ GHz}$, and the terms $d_s/d_{\ell s} = 2$ (i.e., the lens is one-half the distance to the source, which maximizes the geometrical term) and $d_\ell d_{\ell s}/d_s = 1 \text{ Gpc}$. The white regions illustrate the parameter space where refraction produces less than two images and, therefore, there is no scattering, scatter broadening or an effect on scintillation. The blue and red dashed vertical lines delimit the ranges of density values inferred for L^* galaxies at $z \sim 0.2$ from COS-Halos by [Werk et al. 2014](#) and [Prochaska et al. 2017](#), and for massive quiescent galaxies at $z \sim 0.4$ from COS-LRG by [Zahedy et al. 2019](#) (the red lines limit the region containing 68% of the volume density values estimated from their sample; see also [Chen et al. 2023](#))⁶, respectively. Finally, the thick gray diagonal lines

⁵ In reality, the lens will always be at $z > 0$, but we have assumed this value here for simplicity.

⁶ The cloud sizes and densities may be linked to the volume filling fraction, but given the large uncertainties in these parameters we here treat them as independent from each other for visualization.

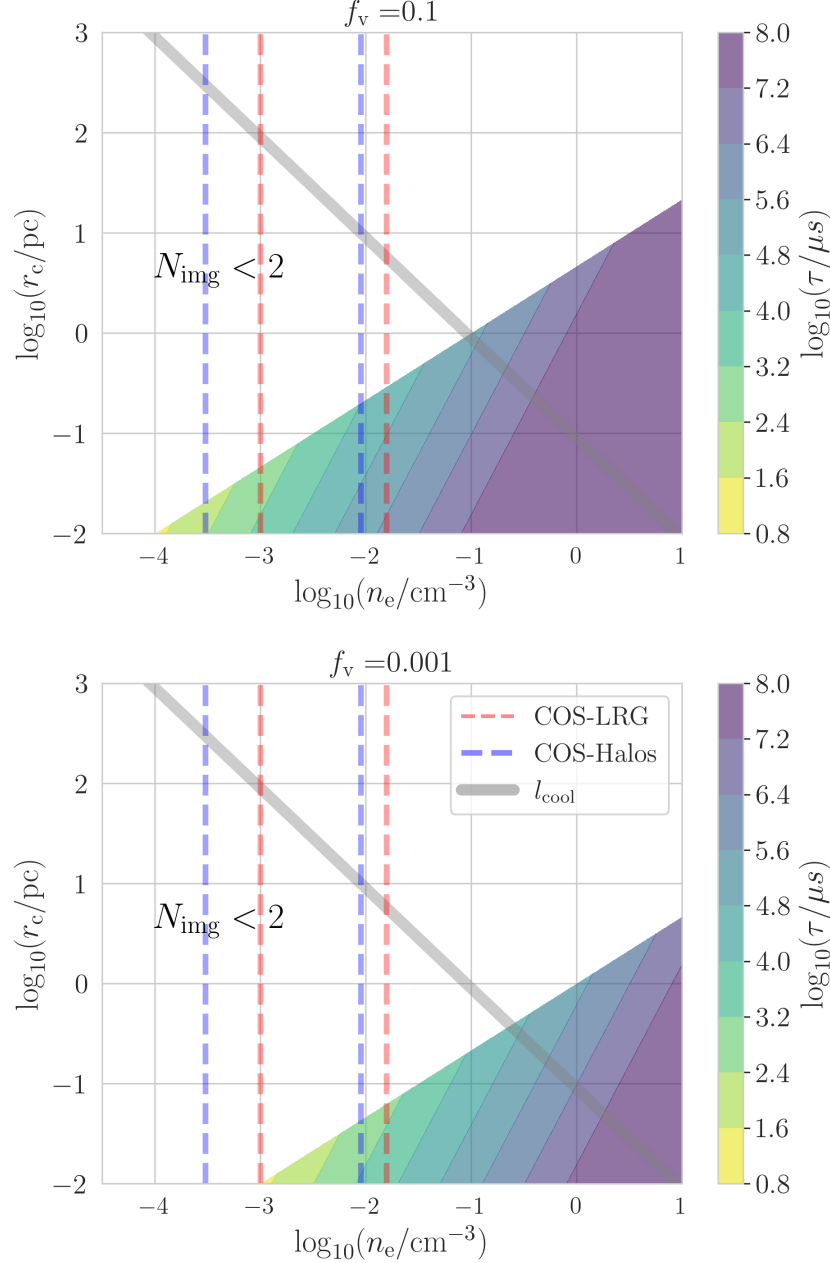


Figure 1. Refractive scattering time delay produced by a halo composed of an ensemble of single-size clouds of radius r_c , electron density n_e , and two volume filling fraction values following Equations 14 and 15. We fix the parameters $z_\ell = 0$, $r_{200} = 200$ kpc, $d_s/d_\ell = 2$, $d_\ell d_\ell/d_s = 1$ Gpc, and an observed frequency of 1 GHz. The white regions indicate the parameter space where refraction in the halo produces less than two images and, thus, does not result in scattering. The vertical blue and red dashed lines express the range of electron density values inferred by Werk et al. (2014) and Prochaska et al. (2017) from COS-Halos data at $z \sim 0.2$, and from the COS-LRG sample at $z \sim 0.4$ in Zahedy et al. (2019), respectively. The thick gray diagonal lines represent the shattering scale from McCourt et al. (2018). Overall, refraction from the bulk of low-density cool CGM gas does not contribute to scattering. Dense gas clumps, however, produce strong scattering that may result in the suppression of Milky Way scintillation.

represent the minimum cooling (shattering) cloud size proposed by [McCourt et al. \(2018\)](#), assuming a fully ionized gas. This scale depends on density as ([Faerman & Werk 2023](#), their equation 15)

$$l_{\text{cool}} \approx 9 \text{ pc} \left(\frac{n}{10^{-2} \text{ cm}^{-3}} \right)^{-1}, \quad (18)$$

for a typical cool gas temperature of 10^4 K , and where n is the total gas density.

Overall, Figure 1 illustrates two important results: First, the CGM gas covering most of the assumed parameter space (large, low density clouds) produces no scattering because its refraction does not produce two images. Second, the halo may produce substantial scattering and suppress scintillation only if the cloud size at CGM densities of $n_e \lesssim 10^{-2} \text{ cm}^{-3}$ is $r_c \lesssim 0.2 \text{ pc}$. Such gas clouds, however, would be approximately 100 times smaller than the shattering scale. If one adopts the shattering scale as a lower limit to the cloud size at a given density, then scattering by the halo (where $N_{\text{img}} \geq 2$) would require pockets of gas at high densities, $n_e \gtrsim 10^{-1} \text{ cm}^{-3}$, which may indeed coexist with the low-density gas in the CGM (e.g., [Chen et al. 2010](#); [Rubin et al. 2011](#); [Putman et al. 2012](#); [Nielsen et al. 2013](#); [Lan & Fukugita 2017](#)). At these high densities, the halo produces multiple ($10 - 100$; Equation 17) images and the time delays are $\tau_s \gtrsim 10 \text{ ms}$, in agreement with the results by [Jow et al. 2023](#), but the detection of such highly scattered FRBs may be challenging. Furthermore, at the highest scattering times, the time delay between images may be larger than the pulse duration and thus these may appear as separated pulses, adding to the complexity for detecting and characterizing such FRBs.

In summary, refraction by cool gas clouds with densities $n_e < 10^{-2} \text{ cm}^{-3}$ in halos will produce only a single image ($N_{\text{img}}=1$) and therefore not result in scattering. No additional constraint may be extracted for such gas from FRB scintillation. However, a population of high density clumps embedded in the halo may yield $N_{\text{img}} > 1$ and result in the significant scattering. We assess the scenario of these dense clumps in more detail in Section 4.3.

Figure 3 in the Appendix shows the same results as Figure 1 but at 400 MHz, the minimum frequency of the CHIME experiment ([CHIME/FRB Collaboration et al. 2018](#)), for comparison and to visualize the effect of the strong dependence on frequency by, both, the number of images and the time delay. Overall, there is a slight increase in the parameter space where $N_{\text{img}} \geq 2$, as well as higher time delays. Owing to the strong ν^{-4} frequency dependence of the number of images, Equation 17 yields about 2 (100) images at a frequency of 400 (100) MHz, with time delays of $\tau_s \approx 0.1(24) \text{ s}$ (Equation 16), which possibly makes these highly-scattered FRBs challenging to detect at these frequencies.

4. PHYSICALLY-MOTIVATED HALO GAS MODELS

We explore now physically-motivated halo models and compare them to our previous results. In particular, we make use of estimates of the dispersion measure in

local halos in Section 4.1, and consider the case of a distribution of cloud sizes in Section 4.2. Dense gas clouds are addressed in Section 4.3, and the constraining power from the presence of scattering in high-redshift proto-cluster structures is investigated in Section 4.4. We finally apply our refractive formalism to two science cases in Sections 4.5 and 4.6.

4.1. An Empirical Halo Model

Prochaska & Zheng (2019) examined a variety of empirical and numerical models that parameterize the ionized gas in local galaxy halos and, assuming a Milky Way halo mass and a single-component model for the halo gas, they showed that the electron density radial profiles from most models broadly agree to within one order of magnitude (their figure 1). In particular, the models show values for the electron number density within the range $n_e = 10^{-3} - 10^{-4} \text{ cm}^{-3}$, from a few tens to about 150 kpc from the center of the halos, and electron columns on the order of $\text{DM} = 100 \text{ pc cm}^{-3}$. We incorporate in our formalism the dispersion measure observable, commonly used in the FRB field, through

$$\text{DM} = N_c \text{DM}_c = 3f_v r_{200} n_e , \quad (19)$$

where $\text{DM}_c = 2r_c n_e$ is the dispersion measure of one cloud intersected through its center. We can now rewrite equations 16 and 17 with this parameter and solve for the maximum cloud size that produces two images, resulting in

$$r_c^3 \approx \frac{(0.12 \text{ pc})^3}{(1+z_\ell)^4} \left(\frac{d_\ell d_{\ell s}/d_s}{1 \text{ Gpc}} \right)^2 \times \left(\frac{\text{DM}}{100 \text{ pc cm}^{-3}} \right) \left(\frac{n_e}{10^{-2} \text{ cm}^{-3}} \right) \left(\frac{1}{N_{\text{img}} - 1} \right) \left(\frac{\nu}{1 \text{ GHz}} \right)^{-4} , \quad (20)$$

with a corresponding refractive scattering time delay of

$$\tau_s \approx \frac{7}{(1+z_\ell)^3} \text{ms} \left(\frac{d_\ell d_{\ell s}/d_s}{1 \text{ Gpc}} \right) \left(\frac{\text{DM}}{100 \text{ pc cm}^{-3}} \right) \times \left(\frac{n_e}{10^{-2} \text{ cm}^{-3}} \right) \left(\frac{r_c}{0.12 \text{ pc}} \right)^{-1} \left(\frac{\nu}{1 \text{ GHz}} \right)^{-4} \quad \text{if} \quad N_{\text{img}} \geq 2 , \quad (21)$$

Here above we have considered $n_e = 10^{-2} \text{ cm}^{-3}$, which is higher than the values estimated by Prochaska & Zheng (2019). This is because these authors considered a single (hot) component that dominates the gaseous halo mass, while the cool, ionized gas that we are interested in is expected to have higher densities (e.g., in pressure equilibrium). We have adopted the DM value as is in Prochaska & Zheng (2019), however, because their value is consistent with those inferred for intervening halos by Khrykin et al. (2024). Our results scale with the values of these parameters as expressed by the above equations.

Consistent with the results in the previous general case, with this set of parameters we overall find that the cloud sizes must be smaller than $r_c \lesssim 0.1$ pc for the halo to produce multiple refractive images and scattering at millisecond scales.

4.2. *A Distribution of Cloud Sizes*

Instead of an ensemble of single-size clouds, we here adopt a distribution of cloud sizes following the results by [Gronke et al. \(2022\)](#) and [Tan & Fielding \(2024\)](#). These authors performed simulations of survival and growth of gas clouds in multiphase media resembling the CGM, and found that the mass distribution of clouds can be described by a power law of the form $dn/dm \propto m^{-2}$, where n now denotes the number of clouds in the distribution, down to the shattering scales of [McCourt et al. \(2018\)](#). By assuming a spherical shape and the same density for all of the clouds, we can rewrite the previous distribution with the cloud radius as $\frac{dn}{dr_c} = \frac{dn}{dm} \frac{dm}{dr_c} \propto r_c^{-4}$, which we adopt for our model.

For this continuous distribution, the scattering angle now becomes (see the full derivation in Section B),

$$\alpha^2 \approx g_s^2 \int_{N_c} \alpha_c^2 = g_s^2 \frac{9}{4} f_v \frac{r_{200}}{r_{c,\min}} \Delta m^2, \quad (22)$$

where $r_{c,\min}$ is the minimum cloud size in the distribution. Here we have ignored the terms containing the maximum cloud size, owing to the steep slope of the distribution and assuming that the two limits differ by a substantial ($\gtrsim 1$ dex) amount. With this expression, the scattering time delay is now

$$\tau_s \approx \frac{1}{(1+z_l)^3} \frac{d_l d_{ls}}{d_s} g_s^2 \frac{9}{8c} f_v \frac{r_{200}}{r_{c,\min}} \Delta m^2. \quad (23)$$

This equation is equivalent to Equation 14 above, but replacing the cloud size there for the minimum cloud size in the distribution here. The preceding factors, however, are not equal in these expressions for the two halo models. Because some of the clouds are larger than the minimum cloud size in the distribution scenario, the total number of clouds is smaller than in the case where all the clouds have the same size and this size equals the minimum cloud radius. This, in turn, reduces the number of transitions between media for the radio waves and, thus, the scattering time. Overall, the distribution of cloud sizes results in a reduction of the scattering time delay by a factor $\left(\frac{\beta-1}{\beta}\right)$ compared to the single-size case (Section B), where $\beta = 4$ is the fiducial power-law index of the distribution adopted here. For the number of images in the scenario with a size distribution, we have that (Section B),

$$N_{\text{img}} - 1 \approx \frac{1}{(1+z_\ell)^4} \left(\frac{d_\ell d_{\ell s}}{d_s}\right)^2 \Delta m^2 \frac{3}{2} f_v \frac{r_{200}}{r_{c,\min}^3}, \quad (24)$$

when $\beta = 4$, corresponding to a reduction in the number of images by a factor $\left(\frac{\beta-1}{\beta+2}\right)$ compared to the single-size case. For smaller values of β , the differences between the

two halo models grow larger, as expected from having a flatter distribution of sizes, i.e., an increased fraction of large clouds. We recall that these expressions are only valid for steep distributions; one should take into account the terms containing the maximum cloud size for the case of distributions with small β values.

In summary, for a halo consisting of a (steep) distribution of cloud sizes following a power law with index β , the time delay and number of images are reduced by factors $\left(\frac{\beta-1}{\beta}\right)$ and $\left(\frac{\beta-1}{\beta+2}\right)$, respectively, compared to the single-size cloud case where this cloud size equals the minimum size of the clouds in the distribution. For $\beta = 4$ obtained from simulations, these terms correspond to factors 3/4 and 1/2, respectively, the latter further contributing to the small number of images expected for the bulk of CGM gas.

4.3. Dense Gas Clumps Near Galaxies

In previous sections we found that when adopting the low density values characteristic of cool gas in the circumgalactic medium of low-redshift halos, refraction from one halo generally does not create two images and, therefore, does not produce scattering. A fraction of dense $n_e \gtrsim 0.1 \text{ cm}^{-3}$ gas, however, may be expected to also co-exist in the central regions of the CGM and, as illustrated in Figure 1, intersecting a number of these dense clumps⁷ can result in substantial scattering.

We now estimate the probability of finding this dense ($n_e \gtrsim 0.1 \text{ cm}^{-3}$) gas along FRB sightlines. Specifically, the probability of intersecting dense clumps can be written as

$$p_{\text{cl}} = \bar{n}_{\text{d}} f_{\text{c}} , \quad (25)$$

where f_{c} is the areal covering fraction of dense (clumpy) gas in a region within a radius from the center of a halo, and

$$\bar{n}_{\text{d}}(z_{\text{FRB}}) = \int_0^{z_{\text{FRB}}} (1+z)^2 d_{\text{H}}(z) \int \pi r_d^2 \frac{dn_{\text{h}}}{dM_{\text{h}}}(z) dM_{\text{h}} dz \quad (26)$$

is the mean number of regions hosting dense clumps along the sightline of an FRB at redshift z_{FRB} (Padmanabhan 2002). Here, $dn_{\text{h}}/dM_{\text{h}}$ is the comoving number density of halos of mass M_{h} , and the term $d_{\text{H}}(z) = c H_0^{-1} [\Omega_{\Lambda} + \Omega_{\text{m}}(1+z)^3]^{-1/2}$, with H_0 , Ω_{Λ} , and Ω_{m} denoting the Hubble constant, and the dark energy and matter densities today, respectively. The parameter $r_d = 10 \text{ kpc}$ determines the radius out to which the dense gas may be expected to reside. This distance is motivated by the fact that we do not expect clouds with $n_e \gtrsim 0.1 \text{ cm}^{-3}$ – the approximate density at which the shattering scale becomes small enough for multiple images – at significant distances from Milky Way like galaxies given that photoionized gas in the interstellar medium has $n_e \sim 1 \text{ cm}^{-3}$. Additionally, as noted in Section 1, $r_d = 10 \text{ kpc}$ corresponds to typical distances to complexes of high velocity clouds (Wakker et al. 2008), estimated to often have densities of $n_e \sim 0.1 \text{ cm}^{-3}$ like those considered here.

⁷ We use the word clump instead of cloud here to differentiate these high density media from the ones considered before.

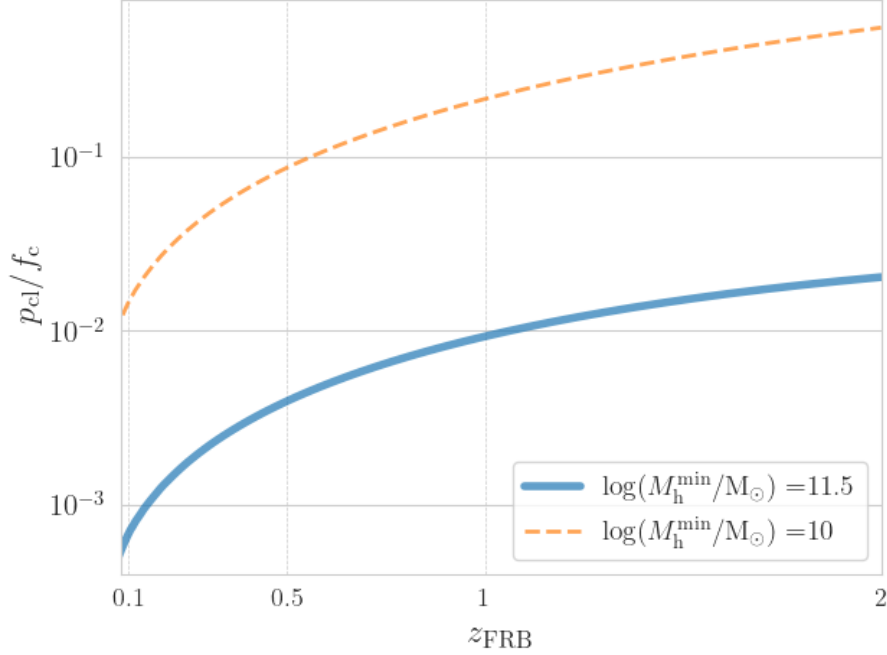


Figure 2. Probability of intersecting dense ($n_e \gtrsim 0.1 \text{ cm}^{-3}$) clumps within the inner 10 kpc of intervening halos along the sightline of a redshift z_{FRB} FRB, which may result in refractive scattering, over the (unknown) covering fraction of this gas in such a central region. The solid blue line denotes halos of mass $\log(M_h/M_\odot) \geq 11.5$, which are the most likely to host cold gas, and the dashed orange line represents halo masses $\log(M_h/M_\odot) \geq 10$ for comparison. Overall, a small fraction of low-redshift ($z \lesssim 0.5$) FRBs are expected to show refractive scattering from this dense gas given the small probabilities of intersecting such regions.

Figure 2 displays the probability of intersecting dense clumps along the sightline of an FRB at redshift z_{FRB} over the (unknown) covering fraction of such dense gas within the inner 10 kpc of halos⁸. This quantity simply corresponds to the mean number of regions hosting dense gas along an FRB sightline (Equation 25). For these calculations, we have used the Tinker et al. 2008 halo mass function from the `hmf` package (Murray et al. 2013), integrated up to the default upper halo mass limit of $\log(M_h^{\text{max}}/M_\odot) = 15$, although this exact value has little impact on the results. The solid blue line denotes a minimum halo mass limit of $\log(M_h^{\text{min}}/M_\odot) = 11.5$, as halo masses near that of the Milky Way are the most efficient at forming stars and hosting cold gas. The dashed orange line corresponds to the case $\log(M_h^{\text{min}}/M_\odot) = 10$, down to small dwarf galaxies, for comparison, although such small halos are unlikely to have cold dense gas. Overall, we anticipate a small fraction of bursts showing refractive scattering from this dense gas. When this happens, it is likely that the FRB sightline passes close to a galaxy, and the images are expected to be separated by milliseconds, if not longer, at $\nu \sim 1 \text{ GHz}$ (Equation 16).

⁸ Although we do not write it explicitly for simplicity, we note that the covering fraction is expected to depend on halo properties and redshift, where over order-unity differences with redshift are likely to occur as we expect denser CGMs at higher redshifts (e.g., Lan & Fukugita 2017; Dutta et al. 2020; Lan 2020).

4.4. $z \gtrsim 2$ Proto-clusters around Quasars

During the last few decades, there have been numerous detections and detailed studies of large (hundreds of kpc across) and dense ($n_{\text{H}} \sim 1 \text{ cm}^{-3}$) environments at redshift $z \gtrsim 2$ with overdensities suggesting they constitute the cool gas component of the progenitors of present-day galaxy clusters (e.g., Steidel et al. 2000; Cantalupo et al. 2014; Hennawi et al. 2015; Geach et al. 2016; Cai et al. 2018; Li et al. 2024). We explore here the gas constraints that can be obtained from the scenario of an FRB behind one of these proto-clusters.

The discovery of one of these massive structures at $z \approx 2$ was reported by Hennawi et al. (2015). These authors examined the nebular emission from the gas, as well as the absorption signature imprinted by this gaseous environment in the spectrum of a background quasar at an impact parameter of 176 kpc from the center of the proto-cluster. From photoionization modeling, Hennawi et al. (2015) inferred hydrogen volume and column densities of $n_{\text{H}} \approx 2 \text{ cm}^{-3}$ and $\log(N_{\text{H}}/\text{cm}^{-2}) = 20.4 \pm 0.4$, respectively, and an ionization fraction of $\sim 90\%$.

Given the large ionization fraction inferred by (Hennawi et al. 2015), for our calculations we simply assume $\log(N_{\text{e}}/\text{cm}^{-2}) = 20.4 \pm 0.4$, which corresponds to $\text{DM} \approx 84_{-51}^{+126} \text{ pc cm}^{-3}$, and $n_{\text{e}} = 2 \text{ cm}^{-3}$, as well as that all this gas (DM) contributes to scattering. Introducing these values into Equation 20, the limiting (maximum) cloud size value to obtain at least two images is $r_{\text{c}} \approx 0.15_{-0.04}^{+0.05} \text{ pc}$, which yields a time delay at 1 GHz of $\tau_{\text{s}} \approx 34_{-10}^{+15} \text{ ms}$. These two values are of the same order as those we obtained for the low-redshift cases despite the high gas density involved in this scenario, due to the strong redshift dependencies of the number of images and time delay. However, contrary to the low-redshift case, scattering from high- z proto-cluster cases may be used to probe the shattering scales, because the maximum cloud size required for scattering found here is similar to the shattering scale expected at these high densities (Equation 18).

Similar to the previous section, we can further assess the probability of intersecting proto-cluster structures along an FRB sightline. By comparing the sizes of the observed area in Hennawi et al. (2015) and around 29 quasars in Hennawi & Prochaska (2013), as well as the extent to where the emission from the proto-cluster gas was detected, Hennawi et al. (2015) argued that about $f_{\text{qso}} = 10\%$ of $z \sim 2$ quasars may have extended gas structures like the one discussed here, with a gas covering fraction of $f_{\text{c,proto}} \sim 30\%$ out to $r_{\text{proto}} \sim 150 \text{ kpc}$ (section 7 in Hennawi et al. 2015). Furthermore, by adopting the quasar luminosity function of Hopkins et al. (2007) down to an apparent magnitude limit of $V = 24$, as well as an obscuration fraction value of 50% consistent with Reyes et al. (2008) and Lusso et al. (2013), Hennawi et al. (2015) derived a mean comoving number density of quasars at $z \sim 2$ of $n_{\text{qso}} = 3.8 \times 10^{-5} \text{ cMpc}^{-3}$. With this information we can now write the probability of intersecting (at least) one proto-cluster along an FRB sightline as (Mas-Ribas &

Dijkstra 2016)

$$p_{\text{proto}} = 1 - (1 - f_{\text{c,proto}})^{\bar{n}_{\text{proto}}} , \quad (27)$$

where $(1 - f_{\text{c,proto}})^{\bar{n}_{\text{proto}}}$ is the probability of not finding any proto-cluster in any of the \bar{n}_{proto} quasars hosting them, and where the probability of intersecting the proto-cluster in one host quasar is given by the areal covering fraction of the proto-cluster gas, $f_{\text{c,proto}}$. Following Equation 26, the mean number of quasars hosting proto-clusters is

$$\bar{n}_{\text{proto}}(z_{\text{FRB}}) = \pi r_{\text{proto}}^2 f_{\text{qso}} n_{\text{qso}} \int_2^{z_{\text{FRB}}} (1+z)^2 d_H(z) dz , \quad (28)$$

where we assume that all proto-cluster structures are well-characterized by the aforementioned $z \sim 2$ parameter values in any case, including the mean number density of quasars, and that proto-clusters exist only at $z \geq 2$. Solving the above equations we find a probability of intersecting a proto-cluster with an FRB sightline of $p_{\text{proto}} \approx 10^{-3}$ ($p_{\text{proto}} \approx 10^{-4}$) at $z_{\text{FRB}} \approx 3$ ($z = 2.1$). This indicates that a future large ($\gtrsim 1000$) sample of $z \gtrsim 3$ FRBs may enable probing the shattering scale and setting further constraints on high-redshift CGM gas.

4.5. Science Case 1: FRB20221219A

Faber et al. (2024) recently reported the discovery of the potentially highly scattered FRB20221219A at $z = 0.55$, whose “overcrowded” sightline traverses two extragalactic halos and the outskirts of a galaxy cluster. These authors measured a scattering timescale from the pulse broadening of $\tau = 19.2$ ms at 1.4 GHz, although they were not able to determine if it had the characteristic $\sim \nu^{-4}$ frequency dependence to help distinguish scattering from the intrinsic width of the FRB. They argued, based on the observed large scattering timescale, that an intervening CGMs was more plausible to be the source of scattering than the Milky Way or the FRB host, but scintillation measurements that could confirm that CGM picture were not obtained.

As an application of the formalism developed above, we can now examine the potential contribution of refraction from the intervening halos to scattering. At first glance, such a large scattering time *could* be produced by refractive scattering⁹. However, the geometric term and the DM halo values in Faber et al. (2024) for FRB20221219A are both a factor of about ten smaller than those considered in Equations 20 and 21. For refraction to be able to produce a scattering time of the order of that measured, Equation 21 results in the condition $n_e/r_c \sim 10 \text{ cm}^{-3} \text{ pc}^{-1}$ which, applied to Equation 20 yields a maximum cloud size of $r_c \sim 0.1 \text{ pc}$ to produce two images. Although these results are consistent with shattering scale clouds of $n_e \approx 1 \text{ cm}^{-3}$, gas of such densities is unlikely to inhabit the measured distances of 36 kpc and 43 kpc from the center of the intersected halos as we discussed previously. Smaller-size clouds could produce more images and would require lower gas densities but this would imply

⁹ We note that considering our fiducial 1 GHz frequency yields $\tau_s \approx 74$ ms, and that, specifically, this scattering timescale corresponds to the $1/e$ value from the pulse broadening, while its tail reaches larger times.

cloud scales far below the shattering size. Overall, refractive scattering appears as an unlikely driver of this signal.

4.6. *Science Case 2: FRB20181112*

Contrary to the large scattering time discussed above, we consider now FRB20281112, detected by the Commensal Real-time Australian Square Kilometer Array Pathfinder (ASKAP) Fast Transient survey (CRAFT; [Bannister et al. 2019](#); [Cho et al. 2020](#); [Scott et al. 2023](#)) and analyzed in [Prochaska et al. \(2019\)](#). This FRB shows a total of $DM = 589.27 \text{ pc cm}^{-3}$, a scattering time of $\tau \approx 40 \mu\text{s}$, and a host at $z = 0.4755$. Its sightline intersects a galaxy at $z = 0.3674$, at an impact parameter of 29 kpc, giving a $DM = 50 - 120 \text{ pc cm}^{-3}$. Adopting $DM = 100 \text{ pc cm}^{-3}$ and plugging these values into Equation 21 yields the relation $n_e/r_c \sim 4 \times 10^{-3} \text{ cm}^{-3} \text{ pc}^{-1}$ that, combined with Equation 20 results in a maximum cloud size of $r_c \sim 4 \times 10^{-3} \text{ pc}$. These values arise from the fact that the measured scattering time is very small compared to the millisecond values obtained in our fiducial calculations; the cloud size must be small to produce two images, but to obtain small scattering times the density needs to be even smaller to counterbalance the effect of the cloud size. This places the gas in an unlikely region of the CGM parameter space (beyond the bottom left corner of Figure 1), suggesting that refraction *is not* the main driver of this scattering.

The two cases just discussed above serve as a proof of concept and example applications of our formalism. We are working on statistically applying this approach to a large number of FRBs to connect the fraction of FRBs without scintillation to the average properties of dense gas in halos.

5. REFRACTIVE VS TURBULENT CGM SCATTERING

Turbulence in the CGM may act as another source of scattering that confuses the determination of whether refractive scattering is happening. Furthermore, if turbulence is occurring within the parsec-scale clouds that can produce refractive scattering, it would increase the scattering in small clouds relative to our refractive calculation. Here we consider how the strength of turbulent scattering compares to our refractive scattering in the limit where the turbulent cascade scales in the manner of Kolmogorov turbulence to sub-astronomical unit lengths which, as we discussed in Section 1, requires specific circumstances in order to hold (e.g. [Lithwick & Goldreich 2001](#); [Prochaska et al. 2019](#)).

For subsonic driving with Mach number $\mathcal{M} < 1$, as is most likely in the CGM (and CGM cloud velocity widths limit $\mathcal{M} \lesssim 2$; [Faerman et al. 2024b](#)), the variance of density fluctuations from isothermal turbulence scales as \mathcal{M}^2 on the driving scale, with an $\mathcal{O}(1)$ coefficient that depends on the properties of the driving ([Vazquez-Semadeni 1994](#))¹⁰. The scattering time can be related to the length scale where the phase

¹⁰ Adiabatic turbulence scales as \mathcal{M}^3 and hence the fluctuations are slightly smaller. Adiabatic is more likely (1) for the virialized rather than cold CGM gas or (2) if the driving scale is smaller than the shattering scale.

structure function equals unity, called the diffractive scale, as $\tau_s = \lambda/(2\pi c)(r_F/r_{\text{diff}})^2$, where r_F is the Fresnel scale (c.f. section 2.3 in Prochaska et al. 2019, for definitions and where redshift factors appear). The phase structure functions from Kolmogorov turbulence at a fixed column density N_e in cold gas up to physical constants and an $\mathcal{O}(1)$ coefficient equals $N_{e,d}^2 \mathcal{M}^2 (r/L)^{5/3}$ for diffraction, whereas the structure function of refractive fluctuations from cloudlets, $N_{e,r}^2 (r/r_c)^2$, where the quadratic scaling applies for most cloudlet geometries (c.f. Vedantham & Phinney 2019 and Prochaska et al. 2019). As the total column participating in turbulence $N_{e,d}$ may be different than in the refractive cloudlets $N_{e,r}$, we can define their ratio $R \equiv N_{e,r}/N_{e,d}$. Thus, for turbulence and refractive lensing to produce the same scattering time, the ratios of the structure functions at r_{diff} must be equal:

$$\frac{R^2}{\mathcal{M}^2} \left(\frac{L}{r_c} \right)^{5/3} \left(\frac{r_{\text{diff}}}{r_c} \right)^{1/3} = 1. \quad (29)$$

Let us assume a similar column participating in turbulence as refractive scattering, so $R = 1$, so that our relation can be rewritten as $L/r_c/\mathcal{M}^{6/5} = (r_c/r_{\text{diff}})^{1/5}$. For millisecond scattering times at cosmological distances, $r_{\text{diff}} \sim 10^{12}$ cm (Prochaska et al. 2019; Ocker et al. 2025). We adopt this value, although our conclusions depend weakly on this choice. If to evaluate the r_{diff}/r_c factor we further take $r_c = 0.03$ pc, close to what is required for refraction at CGM densities – although we note that the dependence of our conclusions on (r_{diff}/r_c) is quite weak –, then equation 29 reduces to $L/r_c/\mathcal{M}^{6/5} = 10$. This means that the scattering time delay from turbulence is the same as from refractive scattering by cloudlets when the driving scale of the turbulence is $L \approx 10 r_c$ if $\mathcal{M} = 1$ or when $L \approx r_c$ if $\mathcal{M} = 0.1$.

We can further put a constraint on how much scattering can be enhanced by turbulence by considering the energetics to drive such turbulence throughout all the cold CGM gas. The dissipation time is the turnover time for the largest eddies, which we are setting to be the cloud size. Thus, the energy density dissipated is roughly equal to:

$$\epsilon = \left(\frac{1}{2} \rho v^2 \right) \frac{v}{L}, \quad (30)$$

where v is the velocity of eddies on the driving scale L . If the CGM is composed of small clouds, the natural driving scale is the cloud scale so $L \sim r_c$.

If the turbulence is driven with Mach number \mathcal{M} at the cloud scale, this becomes:

$$\epsilon = \left(\frac{1}{2} \rho \mathcal{M}^2 c_s^2 \right) \frac{\mathcal{M} c_s}{r_c}, \quad (31)$$

where c_s is the sound speed.

The total energy dissipated in the CGM is then $E_{\text{turb}} = \frac{1}{2} \mathcal{M}^3 \rho c_s^3 V_c r_c^{-1}$, where V_c is the total volume of the clouds, and this needs to be less than the energy in galactic feedback. If galactic feedback is dominated by supernova, each supernova has kinetic

energy $E_{\text{SN}} = 10^{51}$ erg and it takes 100 solar masses of stars formed to have one supernova:

$$E_{\text{feedback}} = \frac{E_{\text{SN}} \text{SFR}}{100} = 10^{49} \text{SFR erg yr}^{-1}, \quad (32)$$

where SFR is the star formation rate in solar masses per year. A Milky Way-like galaxy forms about one solar mass a year. If we say the radius of cold gas in the CGM is 100 kpc, consistent with observations (Werk et al. 2016; Faerman et al. 2024a), the volume filling fraction of cold droplets of size r_c is f_v , and the clouds have a density of $\rho = 1.2 m_p n_e$, where m_p is the proton mass and 1.2 the mean molecular weight, then the dissipated energy is:

$$E_{\text{turb}} = 8 \times 10^{49} \text{ erg yr}^{-1} \left(\frac{f_v}{10^{-3}} \right) \left(\frac{n_e}{10^{-2} \text{ cm}^{-3}} \right) \left(\frac{r_c}{1 \text{ pc}} \right)^{-1} \mathcal{M}^3 \left(\frac{T}{1.5 \times 10^4 \text{ K}} \right)^{3/2}. \quad (33)$$

For parsec-scale clouds and $\mathcal{M} \sim 1$, this exceeds the energy in feedback even for a rather small volume filling factor of $f_v \sim 10^{-3}$ and a density like found in the low- z CGM of $n_e \lesssim 10^{-2} \text{ cm}^{-3}$. We could adjust \mathcal{M} to be smaller, but by $\mathcal{M} = 0.1$ the strength of diffractive scattering from turbulence is comparable to refractive scattering from the cloudlet size (Equation 29).

Thus, this energetics argument suggests that turbulence cannot enhance the scattering of parsec-scale clouds by a large factor over our refractive estimates when there are multiple refractive images. While driving turbulence on a larger scale than r_c is possible to avoid this argument, Equation 29 shows that the driving scale of turbulence can only be an order of magnitude larger than our cloud sizes to produce scattering times similar to those produced by refractive scattering and then for $\mathcal{M} = 1$. Since it is the existence of the clouds themselves that offers the cloud scale as a viable driving scale, this suggests that if CGM scattering times like those estimated in this paper are found, it would likely owe to a mist of clouds being present in the CGM, even if some of the scattering is diffractive.

6. CONCLUSION

In this work we have assessed the contribution of extragalactic halos to refractive FRB scattering, and the constraints on the physical properties of the halo gas obtainable from this observable. Our main results can be summarized as follows:

1. Refraction from the bulk of low-redshift circumgalactic gas in extragalactic halos at densities $n_e \lesssim 10^{-2} \text{ cm}^{-3}$ is not likely to impart scattering delays, and hence suppress the Milky Way scintillation, because the sizes of photoionized clouds are likely too large to produce multiple images. To be able to create multiple images in the low-redshift CGM, the gas clouds should be more than a hundred times smaller than the shattering scale predicted by McCourt et al. (2018).

2. Considering the shattering scale as a lower limit for the sizes of low-redshift CGM clouds, the production of scattering requires gas at densities of $n_e \gtrsim 0.1 \text{ cm}^{-3}$. In this case, the refractive time delays are $\gtrsim 1 - 10 \text{ ms}$.
3. While scattering times of $\gtrsim 1 - 10 \text{ ms}$ from low-redshift CGM may complicate the detection of these FRBs owing to the pulse smearing, these long delays may be a unique signature of refractive scattering: We have argued via constraints on galaxy energetics that diffractive (turbulent) scattering from the CGM is unlikely to be able to produce significantly larger scattering times, and so a population of FRBs with very long scattering times would likely be indicative of sub-parsec CGM clouds. Motivated by high-velocity clouds of similar densities ($n_e \gtrsim 0.1 \text{ cm}^{-3}$) that reside within $\sim 10 \text{ kpc}$ from galaxies, we estimate that a small fraction of FRB sightlines are likely to intersect and be affected by such a dense gas.
4. At redshifts $z \sim 2 - 3$ massive (hundreds of kpc across) proto-clusters observed around quasars are the environment most likely to produce scattering if they are inhabited by shattering-scale (0.1 pc) cloudlets. These media contain substantial $n_e \sim 1 \text{ cm}^{-3}$ cool gas, for which shattering-scale clouds yield tens of millisecond scattering delays. A fraction of $\sim 10^{-3}$ high-redshift FRBs sightlines are expected to intersect such environments.
5. Our conclusions about scattering times and the potential for detecting refractive scattering are unchanged when considering empirical dispersion measure estimates for low-redshift halos, as well as when adopting a distribution of halo cloud sizes motivated by numerical simulations.

In conclusion, refractive scattering in intervening low-redshift halos is sensitive to shattering scale clouds of density $n_e \gtrsim 0.1 \text{ cm}^{-3}$, which are only likely to impact a small fraction of FRB sightlines and then only in the picture of ample shattering-scale cloudlets. Clouds at the highest densities ($n_e \gtrsim 1 \text{ cm}^{-3}$) will have an even smaller effect since they are expected to reside in the innermost regions of the CGM. In an upcoming work, we investigate the constraints on such a very dense gas obtainable from the fraction of FRBs with suppressed scintillation in a large sample. More detailed calculations considering multiple screens would benefit from numerical simulations. However, simulations with enough resolution to treat the radiative transfer effect of scattering (e.g., [Pradeep et al. 2025](#)) are not yet implemented within galaxy-scale codes, as this would require the accurate modeling of a large range of physical scales becoming computationally prohibitive. A first approach, beyond simple analytical calculations with more than one screen, may consider a combination of numerical radiative transfer calculations and the analytical modeling of halo gas. Given that the smallest scales of gas in halos are still under debate, a semi-numerical method may allow for extending calculations to multiple intervening halos efficiently, while also capturing the main physical effects in the CGM.

ACKNOWLEDGEMENTS

L.M.R thanks the Radio Astronomy group at Caltech for kind hospitality while part of this work was performed. We are grateful to Kate Rubin for many discussions and performing CGM cloud simulations for our work. We also thank our colleagues Liang Dai, Jakob Faber, Stella Ocker, Andrew Robertson, Dylan Jow, Gwen Rudie, Ilya Khrykin, Mandy Chen, Mawson Sammons, Phil Hopkins, Sachin Pradeep, Cameron Hummels, Fakhri Zahedy, Michael Rauch, Adam Lanman, Nicolas Tejos, Robert Main, Kenzie Nimmo, Calvin Leung, and Clancy James, among others, for useful discussions. Authors L.M.R and J.X.P, as members of the Fast and Fortunate for FRB Follow-up (F4) team, acknowledge support from NSF grants AST-1911140, AST-1910471, and AST-2206490. M.M. acknowledges support from NSF grant 2007012.

REFERENCES

- Armstrong, J. W., Rickett, B. J., & Spangler, S. R. 1995, *ApJ*, 443, 209, doi: [10.1086/175515](https://doi.org/10.1086/175515)
- Augustin, R., Péroux, C., Hamanowicz, A., et al. 2021, *MNRAS*, 505, 6195, doi: [10.1093/mnras/stab1673](https://doi.org/10.1093/mnras/stab1673)
- Bannister, K. W., Deller, A. T., Phillips, C., et al. 2019, *Science*, 365, 565, doi: [10.1126/science.aaw5903](https://doi.org/10.1126/science.aaw5903)
- Baptista, J., Prochaska, J. X., Mannings, A. G., et al. 2023, Measuring the Variance of the Macquart Relation in z-DM Modeling. <https://arxiv.org/abs/2305.07022>
- Bhardwaj, M., Michilli, D., Kirichenko, A. Y., et al. 2023, Host Galaxies for Four Nearby CHIME/FRB Sources and the Local Universe FRB Host Galaxy Population. <https://arxiv.org/abs/2310.10018>
- Cai, Z., Hamden, E., Matuszewski, M., et al. 2018, *ApJL*, 861, L3, doi: [10.3847/2041-8213/aacce6](https://doi.org/10.3847/2041-8213/aacce6)
- Cantalupo, S., Arrigoni-Battaia, F., Prochaska, J. X., Hennawi, J. F., & Madau, P. 2014, *Nature*, 506, 63, doi: [10.1038/nature12898](https://doi.org/10.1038/nature12898)
- Chen, H.-W., Helsby, J. E., Gauthier, J.-R., et al. 2010, *ApJ*, 714, 1521, doi: [10.1088/0004-637X/714/2/1521](https://doi.org/10.1088/0004-637X/714/2/1521)
- Chen, H.-W., Qu, Z., Rauch, M., et al. 2023, *ApJL*, 955, L25, doi: [10.3847/2041-8213/acf85b](https://doi.org/10.3847/2041-8213/acf85b)
- CHIME/FRB Collaboration, Amiri, M., Bandura, K., et al. 2018, *ApJ*, 863, 48, doi: [10.3847/1538-4357/aad188](https://doi.org/10.3847/1538-4357/aad188)
- Cho, H., Macquart, J.-P., Shannon, R. M., et al. 2020, *ApJL*, 891, L38, doi: [10.3847/2041-8213/ab7824](https://doi.org/10.3847/2041-8213/ab7824)
- Connor, L., Ravi, V., Sharma, K., et al. 2024, arXiv e-prints, arXiv:2409.16952, doi: [10.48550/arXiv.2409.16952](https://doi.org/10.48550/arXiv.2409.16952)
- Cordes, J. M., & Chatterjee, S. 2019, *ARAA*, 57, 417, doi: [10.1146/annurev-astro-091918-104501](https://doi.org/10.1146/annurev-astro-091918-104501)
- Das, H. K., Choudhury, P. P., & Sharma, P. 2021, *MNRAS*, 502, 4935, doi: [10.1093/mnras/stab382](https://doi.org/10.1093/mnras/stab382)
- Draine, B. T. 2011, *Physics of the Interstellar and Intergalactic Medium*
- Dutta, R., Acebron, A., Fumagalli, M., et al. 2024, *MNRAS*, 528, 1895, doi: [10.1093/mnras/stae048](https://doi.org/10.1093/mnras/stae048)
- Dutta, R., Fumagalli, M., Fossati, M., et al. 2020, *MNRAS*, 499, 5022, doi: [10.1093/mnras/staa3147](https://doi.org/10.1093/mnras/staa3147)
- Eftekhari, T., Dong, Y., Fong, W., et al. 2024, arXiv e-prints, arXiv:2410.23336, doi: [10.48550/arXiv.2410.23336](https://doi.org/10.48550/arXiv.2410.23336)
- Ellison, S. L., Ibata, R., Pettini, M., et al. 2004, *A&A*, 414, 79, doi: [10.1051/0004-6361:20034003](https://doi.org/10.1051/0004-6361:20034003)
- Faber, J. T., Ravi, V., Ocker, S. K., et al. 2024, arXiv e-prints, arXiv:2405.14182, doi: [10.48550/arXiv.2405.14182](https://doi.org/10.48550/arXiv.2405.14182)

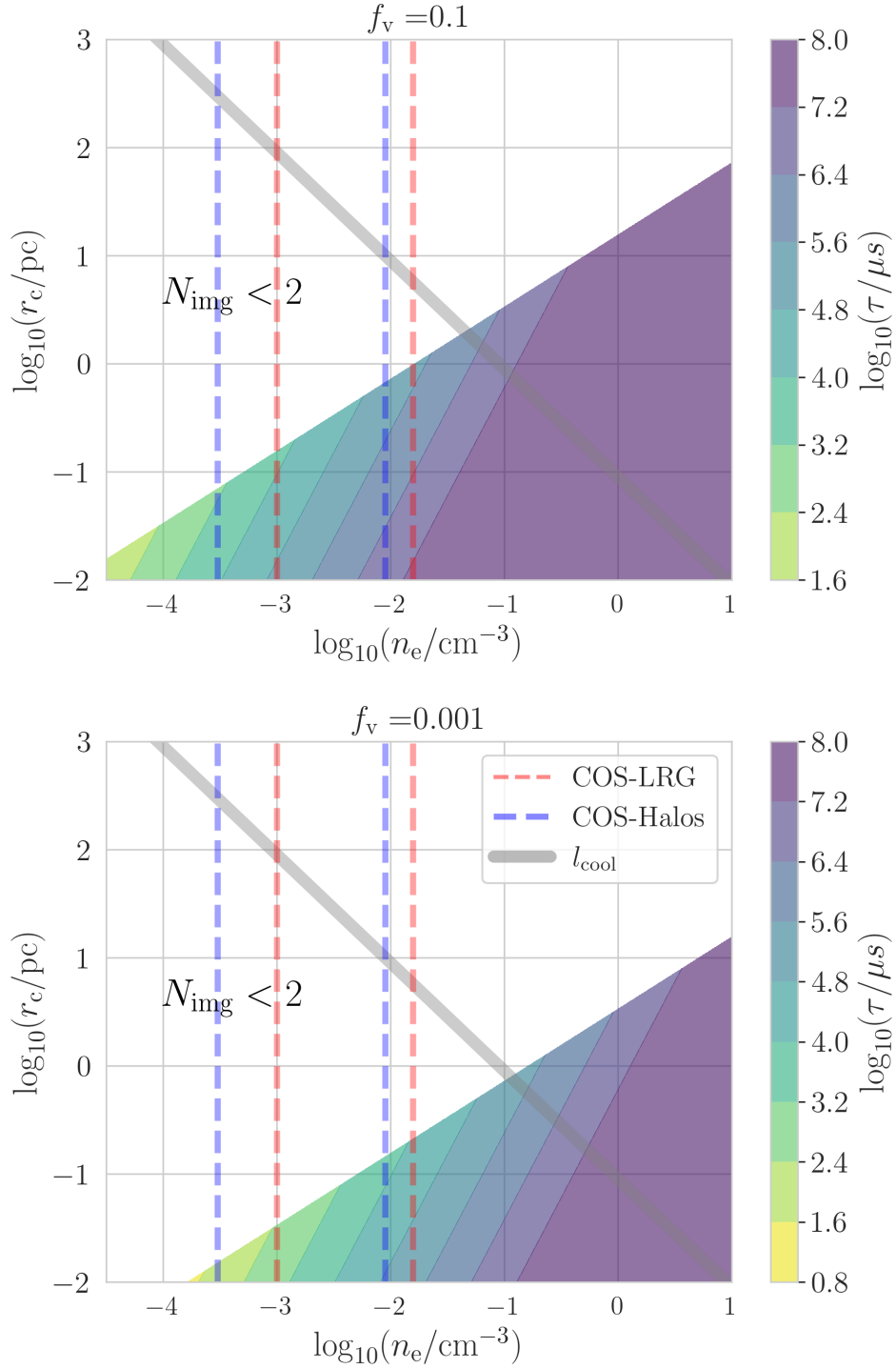
- Faerman, Y., Piacitelli, D. R., McQuinn, M., & Werk, J. K. 2024a, arXiv e-prints, arXiv:2406.03553, doi: [10.48550/arXiv.2406.03553](https://doi.org/10.48550/arXiv.2406.03553)
- . 2024b, arXiv e-prints, arXiv:2406.03553, doi: [10.48550/arXiv.2406.03553](https://doi.org/10.48550/arXiv.2406.03553)
- Faerman, Y., & Werk, J. K. 2023, ApJ, 956, 92, doi: [10.3847/1538-4357/acf217](https://doi.org/10.3847/1538-4357/acf217)
- Farber, R. J., & Gronke, M. 2023, MNRAS, 525, 1839, doi: [10.1093/mnras/stad2373](https://doi.org/10.1093/mnras/stad2373)
- Faucher-Giguere, C.-A., & Oh, S. P. 2023, Key Physical Processes in the Circumgalactic Medium. <https://arxiv.org/abs/2301.10253>
- Geach, J. E., Narayanan, D., Matsuda, Y., et al. 2016, ApJ, 832, 37, doi: [10.3847/0004-637X/832/1/37](https://doi.org/10.3847/0004-637X/832/1/37)
- Ginzburg, V. L. 1970, The propagation of electromagnetic waves in plasmas
- Goldreich, P., & Sridhar, S. 1995, ApJ, 438, 763, doi: [10.1086/175121](https://doi.org/10.1086/175121)
- Gronke, M., & Oh, S. P. 2020, MNRAS, 494, L27, doi: [10.1093/mnrasl/slaa033](https://doi.org/10.1093/mnrasl/slaa033)
- Gronke, M., Oh, S. P., Ji, S., & Norman, C. 2022, MNRAS, 511, 859, doi: [10.1093/mnras/stab3351](https://doi.org/10.1093/mnras/stab3351)
- Hennawi, J. F., & Prochaska, J. X. 2013, ApJ, 766, 58, doi: [10.1088/0004-637X/766/1/58](https://doi.org/10.1088/0004-637X/766/1/58)
- Hennawi, J. F., Prochaska, J. X., Cantalupo, S., & Arrigoni-Battaia, F. 2015, Science, 348, 779, doi: [10.1126/science.aaa5397](https://doi.org/10.1126/science.aaa5397)
- Hewitt, D. M., Bhardwaj, M., Gordon, A. C., et al. 2024, ApJL, 977, L4, doi: [10.3847/2041-8213/ad8ce1](https://doi.org/10.3847/2041-8213/ad8ce1)
- Hopkins, P. F., Richards, G. T., & Hernquist, L. 2007, ApJ, 654, 731, doi: [10.1086/509629](https://doi.org/10.1086/509629)
- Huang, Y.-H., Chen, H.-W., Sheckman, S. A., et al. 2021, MNRAS, 502, 4743, doi: [10.1093/mnras/stab360](https://doi.org/10.1093/mnras/stab360)
- Jow, D. L., Wu, X., & Pen, U.-L. 2023, arXiv e-prints, arXiv:2309.07256, doi: [10.48550/arXiv.2309.07256](https://doi.org/10.48550/arXiv.2309.07256)
- Khrykin, I. S., Ata, M., Lee, K.-G., et al. 2024, ApJ, 973, 151, doi: [10.3847/1538-4357/ad6567](https://doi.org/10.3847/1538-4357/ad6567)
- Kulkarni, V. P., Cashman, F. H., Lopez, S., et al. 2019, ApJ, 886, 83, doi: [10.3847/1538-4357/ab4c2e](https://doi.org/10.3847/1538-4357/ab4c2e)
- Lan, T.-W. 2020, ApJ, 897, 97, doi: [10.3847/1538-4357/ab989a](https://doi.org/10.3847/1538-4357/ab989a)
- Lan, T.-W., & Fukugita, M. 2017, ApJ, 850, 156, doi: [10.3847/1538-4357/aa93eb](https://doi.org/10.3847/1538-4357/aa93eb)
- Lee, K.-G., Ata, M., Khrykin, I. S., et al. 2022, ApJ, 928, 9, doi: [10.3847/1538-4357/ac4f62](https://doi.org/10.3847/1538-4357/ac4f62)
- Lee, K.-G., Khrykin, I. S., Simha, S., et al. 2023, ApJL, 954, L7, doi: [10.3847/2041-8213/acefb5](https://doi.org/10.3847/2041-8213/acefb5)
- Li, M., Zhang, H., Cai, Z., et al. 2024, arXiv e-prints, arXiv:2405.13113, doi: [10.48550/arXiv.2405.13113](https://doi.org/10.48550/arXiv.2405.13113)
- Lithwick, Y., & Goldreich, P. 2001, The Astrophysical Journal, 562, 279, doi: [10.1086/323470](https://doi.org/10.1086/323470)
- Lopez, S., Tejos, N., Ledoux, C., et al. 2018, Nature, 554, 493, doi: [10.1038/nature25436](https://doi.org/10.1038/nature25436)
- Lusso, E., Hennawi, J. F., Comastri, A., et al. 2013, ApJ, 777, 86, doi: [10.1088/0004-637X/777/2/86](https://doi.org/10.1088/0004-637X/777/2/86)
- Macquart, J.-P., & Koay, J. Y. 2013, ApJ, 776, 125, doi: [10.1088/0004-637X/776/2/125](https://doi.org/10.1088/0004-637X/776/2/125)
- Macquart, J.-P., Prochaska, J. X., McQuinn, M., et al. 2020, Nature, 581, 391–395, doi: [10.1038/s41586-020-2300-2](https://doi.org/10.1038/s41586-020-2300-2)
- Mannings, A. G., Fong, W.-f., Simha, S., et al. 2021, The Astrophysical Journal, 917, 75, doi: [10.3847/1538-4357/abff56](https://doi.org/10.3847/1538-4357/abff56)
- Mas-Ribas, L., & Dijkstra, M. 2016, ApJ, 822, 84, doi: [10.3847/0004-637X/822/2/84](https://doi.org/10.3847/0004-637X/822/2/84)
- Masui, K., Lin, H.-H., Sievers, J., et al. 2015, Nature, 528, 523, doi: [10.1038/nature15769](https://doi.org/10.1038/nature15769)
- McCourt, M., Oh, S. P., O’Leary, R., & Madigan, A.-M. 2018, MNRAS, 473, 5407, doi: [10.1093/mnras/stx2687](https://doi.org/10.1093/mnras/stx2687)
- McQuinn, M. 2014, ApJL, 780, L33, doi: [10.1088/2041-8205/780/2/L33](https://doi.org/10.1088/2041-8205/780/2/L33)
- McQuinn, M., & Werk, J. K. 2018, ApJ, 852, 33, doi: [10.3847/1538-4357/aa9d3f](https://doi.org/10.3847/1538-4357/aa9d3f)

- Murray, S. G., Power, C., & Robotham, A. S. G. 2013, *Astronomy and Computing*, 3, 23, doi: [10.1016/j.ascom.2013.11.001](https://doi.org/10.1016/j.ascom.2013.11.001)
- Narayan, R. 1992, *Philosophical Transactions of the Royal Society of London Series A*, 341, 151, doi: [10.1098/rsta.1992.0090](https://doi.org/10.1098/rsta.1992.0090)
- Nielsen, N. M., Churchill, C. W., & Kacprzak, G. G. 2013, *ApJ*, 776, 115, doi: [10.1088/0004-637X/776/2/115](https://doi.org/10.1088/0004-637X/776/2/115)
- Nimmo, K., Pleunis, Z., Beniamini, P., et al. 2024, Magnetospheric origin of a fast radio burst constrained using scintillation. <https://arxiv.org/abs/2406.11053>
- Ocker, S. K., Chen, M., Oh, S. P., & Sharma, P. 2025, arXiv e-prints, arXiv:2503.02329, doi: [10.48550/arXiv.2503.02329](https://doi.org/10.48550/arXiv.2503.02329)
- Padmanabhan, T. 2002, *Theoretical Astrophysics - Volume 3, Galaxies and Cosmology*, Vol. 3, doi: [10.2277/0521562422](https://doi.org/10.2277/0521562422)
- Peacock, J. A. 1999, *Cosmological Physics*
- Pen, U.-L., & Levin, Y. 2014, *Monthly Notices of the Royal Astronomical Society*, 442, 3338, doi: [10.1093/mnras/stu1020](https://doi.org/10.1093/mnras/stu1020)
- Péroux, C., Rahmani, H., Arrigoni Battaia, F., & Augustin, R. 2018, *MNRAS*, 479, L50, doi: [10.1093/mnrasl/sly090](https://doi.org/10.1093/mnrasl/sly090)
- Petroff, E., Hessels, J. W. T., & Lorimer, D. R. 2022, *A&A Rev.*, 30, 2, doi: [10.1007/s00159-022-00139-w](https://doi.org/10.1007/s00159-022-00139-w)
- Pisano, D. J., Barnes, D. G., Gibson, B. K., et al. 2007, *ApJ*, 662, 959, doi: [10.1086/517986](https://doi.org/10.1086/517986)
- Pradeep, S. E., Sprenger, T., Wucknitz, O., Main, R. A., & Spitler, L. G. 2025, arXiv e-prints, arXiv:2505.04576. <https://arxiv.org/abs/2505.04576>
- Prochaska, J. X., & Zheng, Y. 2019, *MNRAS*, 485, 648, doi: [10.1093/mnras/stz261](https://doi.org/10.1093/mnras/stz261)
- Prochaska, J. X., Werk, J. K., Worseck, G., et al. 2017, *ApJ*, 837, 169, doi: [10.3847/1538-4357/aa6007](https://doi.org/10.3847/1538-4357/aa6007)
- Prochaska, J. X., Macquart, J.-P., McQuinn, M., et al. 2019, *Science*, 366, 231, doi: [10.1126/science.aay0073](https://doi.org/10.1126/science.aay0073)
- Putman, M. E., Bland-Hawthorn, J., Veilleux, S., et al. 2003, *ApJ*, 597, 948, doi: [10.1086/378555](https://doi.org/10.1086/378555)
- Putman, M. E., Peek, J. E. G., & Joun, M. R. 2012, *ARAA*, 50, 491, doi: [10.1146/annurev-astro-081811-125612](https://doi.org/10.1146/annurev-astro-081811-125612)
- Qu, Z., Chen, H.-W., Rudie, G. C., et al. 2022, *MNRAS*, 516, 4882, doi: [10.1093/mnras/stac2528](https://doi.org/10.1093/mnras/stac2528)
- Rauch, M., Sargent, W. L. W., Barlow, T. A., & Carswell, R. F. 2001, *ApJ*, 562, 76, doi: [10.1086/323523](https://doi.org/10.1086/323523)
- Reyes, R., Zakamska, N. L., Strauss, M. A., et al. 2008, *AJ*, 136, 2373, doi: [10.1088/0004-6256/136/6/2373](https://doi.org/10.1088/0004-6256/136/6/2373)
- Rickett, B. J. 1970, *MNRAS*, 150, 67, doi: [10.1093/mnras/150.1.67](https://doi.org/10.1093/mnras/150.1.67)
- . 1990, *ARAA*, 28, 561, doi: [10.1146/annurev.aa.28.090190.003021](https://doi.org/10.1146/annurev.aa.28.090190.003021)
- Rubin, K. H. R., Diamond-Stanic, A. M., Coil, A. L., Crighton, N. H. M., & Stewart, K. R. 2018a, *ApJ*, 868, 142, doi: [10.3847/1538-4357/aad566](https://doi.org/10.3847/1538-4357/aad566)
- Rubin, K. H. R., Prochaska, J. X., Ménard, B., et al. 2011, *ApJ*, 728, 55, doi: [10.1088/0004-637X/728/1/55](https://doi.org/10.1088/0004-637X/728/1/55)
- Rubin, K. H. R., O'Meara, J. M., Cooksey, K. L., et al. 2018b, *ApJ*, 859, 146, doi: [10.3847/1538-4357/aaab7](https://doi.org/10.3847/1538-4357/aaab7)
- Rudie, G. C., Steidel, C. C., Pettini, M., et al. 2019, *ApJ*, 885, 61, doi: [10.3847/1538-4357/ab4255](https://doi.org/10.3847/1538-4357/ab4255)
- Ryder, S. D., Bannister, K. W., Bhandari, S., et al. 2023, *Science*, 382, 294, doi: [10.1126/science.adf2678](https://doi.org/10.1126/science.adf2678)
- Sammons, M. W., Deller, A. T., Glowacki, M., et al. 2023, *MNRAS*, 525, 5653, doi: [10.1093/mnras/stad2631](https://doi.org/10.1093/mnras/stad2631)
- Schekochihin, A. A. 2022, *Journal of Plasma Physics*, 88, 155880501, doi: [10.1017/S0022377822000721](https://doi.org/10.1017/S0022377822000721)
- Scott, D. R., Cho, H., Day, C. K., et al. 2023, *Astronomy and Computing*, 44, 100724, doi: [10.1016/j.ascom.2023.100724](https://doi.org/10.1016/j.ascom.2023.100724)

- Shah, V., Shin, K., Leung, C., et al. 2024, arXiv e-prints, arXiv:2410.23374, doi: [10.48550/arXiv.2410.23374](https://doi.org/10.48550/arXiv.2410.23374)
- Sharma, K., Ravi, V., Connor, L., et al. 2024, *Nature*, 635, 61, doi: [10.1038/s41586-024-08074-9](https://doi.org/10.1038/s41586-024-08074-9)
- Simha, S., Burchett, J. N., Prochaska, J. X., et al. 2020, *ApJ*, 901, 134, doi: [10.3847/1538-4357/abafc3](https://doi.org/10.3847/1538-4357/abafc3)
- Simha, S., Lee, K.-G., Prochaska, J. X., et al. 2023, *ApJ*, 954, 71, doi: [10.3847/1538-4357/ace324](https://doi.org/10.3847/1538-4357/ace324)
- Steidel, C. C., Adelberger, K. L., Shapley, A. E., et al. 2000, *ApJ*, 532, 170, doi: [10.1086/308568](https://doi.org/10.1086/308568)
- Stern, J., Hennawi, J. F., Prochaska, J. X., & Werk, J. K. 2016, *ApJ*, 830, 87, doi: [10.3847/0004-637X/830/2/87](https://doi.org/10.3847/0004-637X/830/2/87)
- Stocke, J. T., Keeney, B. A., Danforth, C. W., et al. 2013, *ApJ*, 763, 148, doi: [10.1088/0004-637X/763/2/148](https://doi.org/10.1088/0004-637X/763/2/148)
- Tan, B., & Fielding, D. B. 2024, *MNRAS*, 527, 9683, doi: [10.1093/mnras/stad3793](https://doi.org/10.1093/mnras/stad3793)
- Tejos, N., López, S., Ledoux, C., et al. 2021, *MNRAS*, 507, 663, doi: [10.1093/mnras/stab2147](https://doi.org/10.1093/mnras/stab2147)
- Tinker, J., Kravtsov, A. V., Klypin, A., et al. 2008, *ApJ*, 688, 709, doi: [10.1086/591439](https://doi.org/10.1086/591439)
- Tumlinson, J., Peebles, M. S., & Werk, J. K. 2017, *Annual Review of Astronomy and Astrophysics*, 55, 389–432, doi: [10.1146/annurev-astro-091916-055240](https://doi.org/10.1146/annurev-astro-091916-055240)
- Vazquez-Semadeni, E. 1994, *ApJ*, 423, 681, doi: [10.1086/173847](https://doi.org/10.1086/173847)
- Vedantham, H. K., & Phinney, E. S. 2019, *MNRAS*, 483, 971, doi: [10.1093/mnras/sty2948](https://doi.org/10.1093/mnras/sty2948)
- Vogelaar, M. G. R., & Wakker, B. P. 1994, *A&A*, 291, 557
- Wakker, B. P., & van Woerden, H. 1997, *ARAA*, 35, 217, doi: [10.1146/annurev.astro.35.1.217](https://doi.org/10.1146/annurev.astro.35.1.217)
- Wakker, B. P., York, D. G., Wilhelm, R., et al. 2008, *ApJ*, 672, 298, doi: [10.1086/523845](https://doi.org/10.1086/523845)
- Waters, T., & Proga, D. 2023, *Frontiers in Astronomy and Space Sciences*, 10, 1198135, doi: [10.3389/fspas.2023.1198135](https://doi.org/10.3389/fspas.2023.1198135)
- Werk, J. K., Prochaska, J. X., Thom, C., et al. 2013, *ApJS*, 204, 17, doi: [10.1088/0067-0049/204/2/17](https://doi.org/10.1088/0067-0049/204/2/17)
- Werk, J. K., Prochaska, J. X., Tumlinson, J., et al. 2014, *ApJ*, 792, 8, doi: [10.1088/0004-637X/792/1/8](https://doi.org/10.1088/0004-637X/792/1/8)
- Werk, J. K., Prochaska, J. X., Cantalupo, S., et al. 2016, *ApJ*, 833, 54, doi: [10.3847/1538-4357/833/1/54](https://doi.org/10.3847/1538-4357/833/1/54)
- Williamson, I. P. 1972, *MNRAS*, 157, 55, doi: [10.1093/mnras/157.1.55](https://doi.org/10.1093/mnras/157.1.55)
- Zahedy, F. S., Chen, H.-W., Johnson, S. D., et al. 2019, *MNRAS*, 484, 2257, doi: [10.1093/mnras/sty3482](https://doi.org/10.1093/mnras/sty3482)
- Zahedy, F. S., Chen, H.-W., Cooper, T. M., et al. 2021, *MNRAS*, 506, 877, doi: [10.1093/mnras/stab1661](https://doi.org/10.1093/mnras/stab1661)

APPENDIX

A. CLOUD CONSTRAINTS AT 400 MHZ

**Figure 3.** Same as Figure 1 but at a frequency of 400 MHz.

B. DERIVATION OF THE SCATTERING ANGLE AND NUMBER OF IMAGES FOR A CLOUD-SIZE DISTRIBUTION

For a cloud-size distribution $\frac{dn}{dr_c} \propto r_c^{-4}$, the scattering angle is

$$\begin{aligned} \alpha^2 &\approx g_s^2 \int_{N_c} \alpha_c^2 = 2 g_s^2 N_c \Delta m^2 = 2 g_s^2 \Delta m^2 \frac{\int \frac{dn}{dr_c} 2 \int_0^{\sqrt{r_{200}^2 - b^2}} \frac{\pi r_c^2}{\frac{4}{3} \pi r_c^3} f_v(\sqrt{s^2 + b^2}) ds dr_c}{\int \frac{dn}{dr_c} dr_c} \\ &\approx 3 g_s^2 f_v r_{200} \Delta m^2 \frac{\int \frac{dn}{dr_c} \frac{dr_c}{r_c}}{\int \frac{dn}{dr_c} dr_c} = g_s^2 \frac{9}{4} f_v \frac{r_{200}}{r_{c,\min}} \Delta m^2, \end{aligned} \quad (\text{B1})$$

where we have assumed that the term with the maximum cloud size is negligible compared to the term with the minimum cloud size. For the case of a power law with arbitrary index β , we have

$$\alpha^2 = g_s^2 \frac{3(\beta - 1)}{\beta} f_v \frac{r_{200}}{r_{c,\min}} \Delta m^2. \quad (\text{B2})$$

We can then compute the number of images for the distribution case as

$$\begin{aligned} N_{\text{img}} - 1 &\approx N_c k_c^2 = \frac{1}{(1 + z_l)^4} \left(\frac{d_l d_{ls}}{d_s} \right)^2 \Delta m^2 3 f_v r_{200} \frac{\int \frac{dn}{dr_c} \frac{dr_c}{r_c^3}}{\int \frac{dn}{dr_c} dr_c} \\ &= \frac{1}{(1 + z_l)^4} \left(\frac{d_l d_{ls}}{d_s} \right)^2 \Delta m^2 \frac{3}{2} f_v \frac{r_{200}}{r_{c,\min}^3}, \end{aligned} \quad (\text{B3})$$

and for an arbitrary index β we obtain

$$N_{\text{img}} - 1 \approx \frac{1}{(1 + z_l)^4} \left(\frac{d_l d_{ls}}{d_s} \right)^2 \Delta m^2 \frac{3(\beta - 1)}{(\beta + 2)} f_v \frac{r_{200}}{r_{c,\min}^3}. \quad (\text{B4})$$